



# Transient pressure changes in the vertebral canal during whiplash motion – A hydrodynamic modeling approach



Hua-Dong Yao\*, Mats Y. Svensson, Håkan Nilsson

Chalmers University of Technology, SE-412 96 Gothenburg, Sweden

## ARTICLE INFO

*Article history:*  
Accepted 4 January 2016

*Keywords:*  
Whiplash motion  
Pressure transients  
Internal vertebral venous plexuses  
Dorsal root ganglion  
Neck injury  
Hydrodynamic system of tubes

## ABSTRACT

In vehicle collisions, the occupant's torso is accelerated in a given direction while the unsupported head tends to lag behind. This mechanism results in whiplash motion to the neck. In whiplash experiments conducted for animals, pressure transients have been recorded in the spinal canal. It was hypothesized that the transients caused dorsal root ganglion dysfunction. Neck motion introduces volume changes inside the vertebral canal. The changes require an adaptation which is likely achieved by redistribution of blood volume in the internal vertebral venous plexus (IVVP). Pressure transients then arise from the rapid redistribution. The present study aimed to explore the hypothesis theoretically and analytically. Further, the objectives were to quantify the effect of the neck motion on the pressure generation and to identify the physical factors involved. We developed a hydrodynamic system of tubes that represent the IVVP and its lateral intervertebral vein connections. An analytical model was developed for an anatomical geometrical relation that the venous blood volume changes with respect to the vertebral angular displacement. This model was adopted in the hydrodynamic tube system so that the system can predict the pressure transients on the basis of the neck vertebral motion data from a whiplash experiment. The predicted pressure transients were in good agreement with the earlier experimental data. A parametric study was conducted and showed that the system can be used to assess the influences of anatomical geometrical properties and vehicle collision severity on the pressure generation.

© 2016 Elsevier Ltd. All rights reserved.

## 1. Introduction

Reviews of [Siegmund et al. \(2009\)](#) and [Curatolo et al. \(2011\)](#) concluded that whiplash injury is the most common motor vehicle injury and the most poorly understood. They reviewed potential anatomical injury sites in the neck and listed seven: facet joints, spinal ligaments, intervertebral discs, vertebral arteries, dorsal root ganglia (DRG), neck muscles and vertebral artery. [Cairns et al. \(2015\)](#) pointed to neuroinflammation and glial cell activation in the DRG and spinal cord as a possible mechanism behind the transition from acute pain to chronic pain. This development revives the interest in the DRG as a potential whiplash injury site. Earlier experiments ([Svensson et al., 1998](#); [Örtengren et al., 1996](#)) revealed signs of DRG nerve cell body damage in the cervical and upper thoracic levels after whiplash exposure in a porcine model. [Taylor \(2002\)](#) found that similar, but more severe, DRG injury occurred in cervical spines of victims who had sustained blunt trauma, whereas the surrounding tissues showed no signs of damage.

The experiments ([Örtengren et al., 1996](#); [Svensson et al., 1998](#)) reported remarkable pressure transients in the spinal canal during whiplash motion. These findings supported the hypothesis of [Aldman \(1986\)](#) that changes of the spinal canal volume during sagittal neck motion would cause transient pressure gradients along the canal. The gradients would load and injure the nerve tissue inside the canal. [Eichberger et al. \(2000\)](#) reproduced very similar pressure pulses in postmortem human subjects during staged rear-end collisions. [Panjabi \(2006\)](#) found that during extension of the cervical spine, the intervertebral foramina narrowed, which was exacerbated in individuals with foraminal spondylosis due to smaller bony foraminal dimensions. The narrowed space of the foramen could potentially result in injurious compression of the DRG and is thus an alternative explanation to the DRG injury. [Gustafsson et al. \(2015\)](#) however found the greatest rate of whiplash associated disorders in younger age groups, females aged 30–44 years and males aged 45–59 years, where spondylosis is of minor concern.

[Aldman \(1986\)](#) realized that the spinal canal volume would alter during whiplash motion. He understood that the volume alteration would require a redistribution of the incompressible contents in the canal. Aldman pointed to two fluid systems in the spinal canal, the cerebrospinal fluid (CSF) and the internal vertebral venous plexus (IVVP). He suggested that flow in one or both of these systems would

\* Corresponding author at: Division of Fluid Dynamics, Department of Applied Mechanics, Chalmers University of Technology, SE-41296 Gothenburg, Sweden.  
E-mail address: [huadong@chalmers.se](mailto:huadong@chalmers.se) (H.-D. Yao).

provide volume compensation. Svensson (1993) proposed that the IVVP and intervertebral vein (IV) would be the main contributor to the volume compensation. Fig. 1 shows a diagram of the vertebral vein network in a transverse plane based on an illustration by Breschet (1819). The IVVP lies within the epidural space in the vertebral canal and is supported by a collagenous-fiber network. Its function was described in the works (Batson, 1940; Moore et al., 2013). In contrast to most venous vessels the plexus veins have no valve structures as addressed by Parke et al. (1992), so that the venous blood is free to flow in two directions. The IV connects the IVVP and external vertebral venous plexus (EVVP) via the intervertebral foramen. Batson (1957) reported that it was possible for the blood to flow in both directions inside the IV. However, a challenge is to understand how the volume compensation drives the blood flow in the IVVP and IV and produces the pressure transients.

The objective of the present study was to explore the hypothesis of blood flow. A one dimensional hydrodynamic model including the IVVP and IV was proposed for the hypothesis. Other objectives

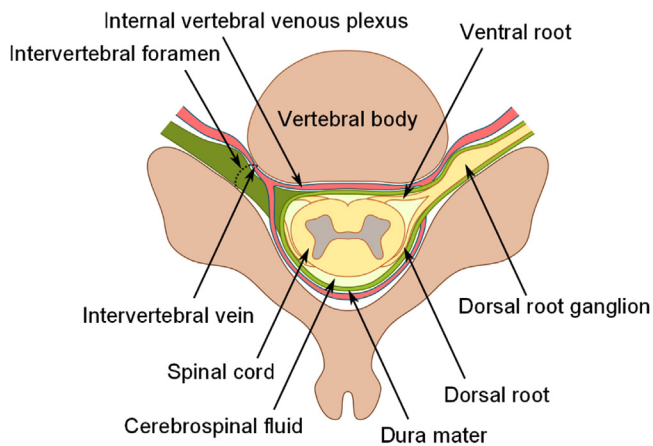


**Fig. 1.** A schematic picture showing a transverse slice of a vertebra in the mid cervical spine. The internal vertebral venous plexus (IVVP) and the intervertebral veins (IV) are drawn in red. The dura mater and its lateral nerve root sleeves are green. The change in spinal canal inner volume during neck motion causes IVVP blood volumes to flow through the IVs. (For interpretation of the references to color in this figure caption, the reader is referred to the web version of this paper.)

were to quantify the impact of the neck motion on the pressure generation and to identify the important anatomical parameters.

## 2. Method

### 2.1. Hypothesis regarding the volume compensation process

A synthesis of literature findings by Svensson (1993) is further developed here. As shown in Fig. 2, the cervical spine elongates during flexion, and shortens during extension (Jonsson, 2008). The volume in the spinal canal therefore increases during flexion, and decreases during extension. Furthermore, Siegmund et al. (1998) found that the canal volume varied between the neutral and retracted neck postures.

Estes and McElhane (1970) reported that all tissues and fluids inside the vertebral canal are virtually incompressible. This means that fluid transportation, to and from the canal, must take place during the flexion-extension motion. The fluid would be either blood or the CSF. Results by Löfgren et al. (1973) indicate that the flow resistance of the CSF in the subdural space of the canal is relatively high. Thus, in this context, the CSF flow may be of minor importance compared with the blood flow. Löfgren's results also show that the pressure imposed for deforming the arteries is higher than that for deforming the CSF volume. Therefore, we assume that the blood transportation in the IVVP is dominant in compensating the canal volume. Nonetheless, the arterial blood can also change the volume and generate pulse waves (Alastruey et al., 2012). Neglecting this effect is a simplification of the present work.

Breig (1978) found that most of the soft tissues in the canal deform in fixed positions during neck motion. Combining the above discussions for the CSF and arterial blood, it is assumed that the volumes of these fluids and soft tissues do not change during flexion and extension. Therefore, if the canal volume varies, the volume filled by the venous blood will change correspondingly.

Fig. 3 illustrates the process of volume compensation by the venous blood flow. It shows a section of the vertebral canal consisting of two vertebral levels. In flexion, the dura sac elongates along the canal and contracts in the horizontal direction. In extension, the dura sac shortens together with a horizontal expansion. Meanwhile, the total volume inside the canal increases in flexion and decreases in extension. The volume changes are compensated by the venous blood.

### 2.2. Formulations

A hydrodynamic model was developed to simulate the volume compensation using Matlab-Simulink produced by MathWorks. Firstly a set of schematic geometrical relations were defined. Then the IVVP and canal were simplified into cylindrical tubes. Fig. 4 illustrates the simplified geometry of two adjacent vertebrae and their relative motion in flexion. The IVVP tube is shown in gray, while the total volume change of the canal is in dark gray. The soft tissues drawn in white remain virtually unchanged during neck motion. In this schematic model, the instant center of rotation of the upper vertebra is located within the vertebral body

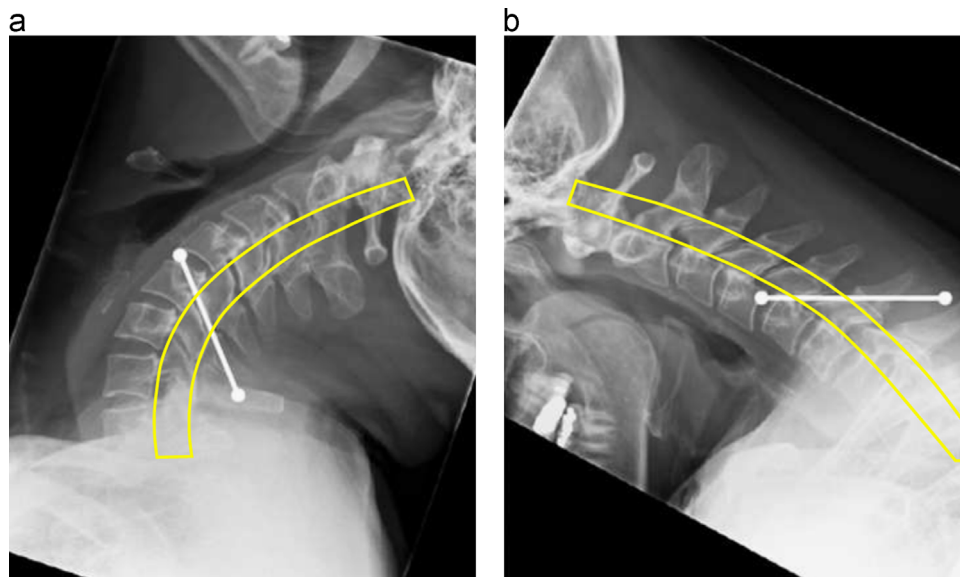


**Fig. 2.** X ray pictures of the cervical spine during (a) extension and (b) flexion. The white line is parallel with the facet joint plane between C5 and C6. The yellow contours enclose the vertebral canal between the head and the C7 vertebra. The vertebral canal is shortened during extension (a) and elongated in flexion (b). Reproduced with permission of Jonsson (2008). (For interpretation of the references to color in this figure caption, the reader is referred to the web version of this paper.)

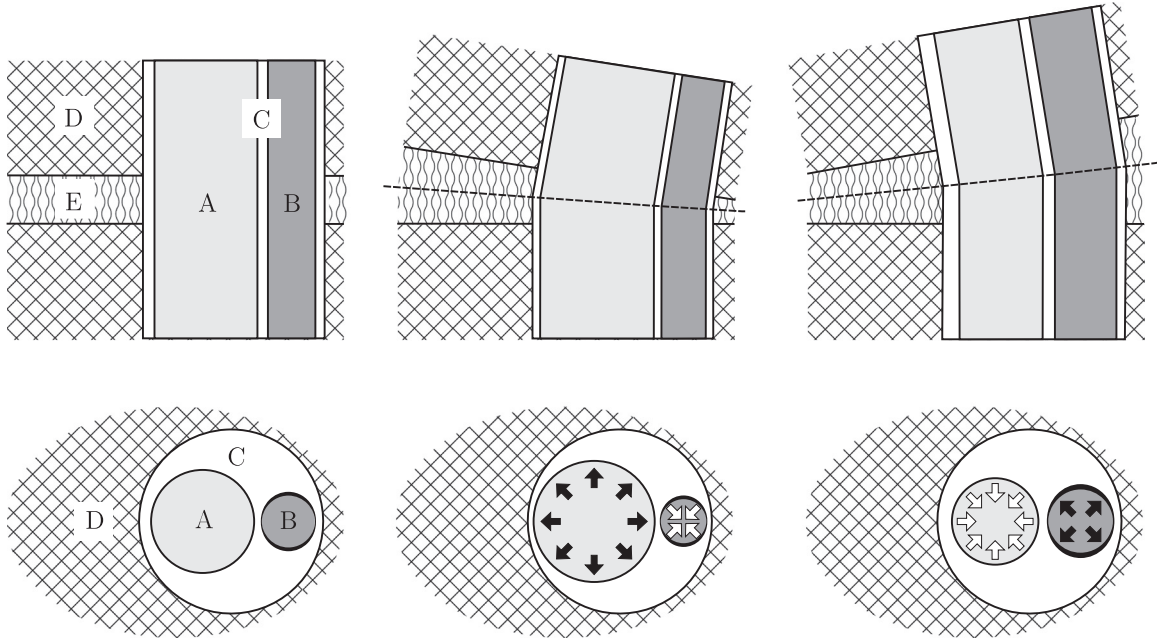


**Fig. 3.** A schematic diagram of the spinal canal with three basic bending types and the corresponding deformations of the soft tissues. From left to right: neutral, extension, and flexion. A: soft tissues, B: internal vertebral venous plexus, C: arteries, D: vertebral body, E: intervertebral disc. White arrows represent contraction, and black arrows expansion.

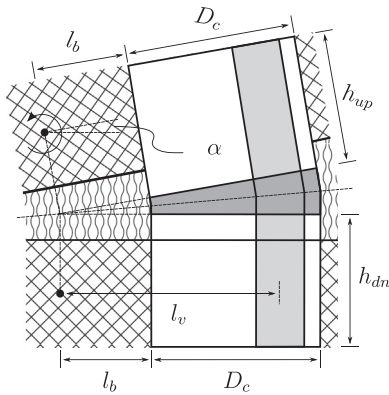


**Fig. 4.** Schematic view of two adjacent vertebrae in flexion, viewed in the sagittal plane. White shows the soft tissues. Gray marks the IVVP. Dark gray shows the expanded canal volume. The black dots represent imaginary the rotation centers.

in contrast to the real human neck where it is located in the body of the inferior vertebra (Penning, 1995). Since the total volume of the posterior veins is higher than that of the anterior veins, the central line of the IVVP tube is placed posterior of the central line of the canal.

The distance from the instant center of rotation to the canal wall is given by

$$l_b = \frac{1}{7} \sum_{i=1}^7 l_{b,i}, \quad (1)$$

where the subscript  $i$  denotes the vertebra number enumerated from the head to torso.  $l_b$  is specified as half of the anteroposterior (AP) diameter of the vertebral body. The sagittal diameter of the canal is defined as

$$D_c = \frac{1}{7} \sum_{i=1}^7 D_{c,i}. \quad (2)$$

The change of the total canal volume is

$$V_c = \frac{\pi D_c^2 \tan(\alpha/2)}{4} (2l_b + D_c), \quad (3)$$

where  $\alpha$  is the difference of the instant rotation angles between the two vertebrae. As  $\alpha = 0$ , the vertebrae stay in the neutral position.

The volume change is assumed to be distributed evenly in the two adjacent vertebral canal sections. It yields

$$V_{c,up} = V_{c,dn} = V_c/2, \quad (4)$$

where the subscripts  $up$  and  $dn$  denotes the upper and lower vertebra.

The distance from the central line of the IVVP tube to the instant center of rotation is

$$l_v = l_b + \frac{1+2\beta}{2} D_c, \quad (5)$$

where  $\beta = l_d/D_c$ .  $l_d$  is the distance from the central line of the IVVP tube to the central line of the canal.

The volume of the IVVP tube is given by

$$V_v = S_v [2 \tan(\alpha/2) l_v + h_{up} + h_{dn}], \quad (6)$$

where  $h$  represents the neutral-position canal length that is equal to the vertebral height, and  $S_v$  is the cross-sectional area of the IVVP tube.

Due to the compensation effect, the volume change of the IVVP tube satisfies

$$\frac{dV_v}{dt} = \frac{dV_c}{dt}. \quad (7)$$

Substituting Eqs. (6) and (3) into Eq. (7),

$$\left[ l_v \sec^2(\alpha/2) \frac{d\alpha}{dt} \right] S_v + [2l_v \tan(\alpha/2) + h_{up} + h_{dn}] \frac{dS_v}{dt} = \frac{\pi D_c^2 (2l_b + D_c)}{8} \sec^2(\alpha/2) \frac{d\alpha}{dt}. \quad (8)$$

The derivation for the volume in the extension is identical to that in the flexion as shown above. Therefore, for brevity, the derivation is not described herein. It is worth noting that extension results in a squeezing effect of the venous blood, while flexion causes a suction effect.

According to Eq. (8), the IVVP tube dynamically adapts the volume by changing both of the length and diameter. However, this adaption can bring some modeling difficulties such as wall boundary conditions and a deforming computational domain. To solve the problem, an approximation adopted is that the volume change of the tube can be transformed into the mass flow in it without changing the length and diameter, based on the equivalence rule of Reynolds number  $Re$ , in which flow with the same  $Re$  possesses equivalent features. Then, the mass flow satisfies

$$(Re)_{fz} = (Re)_{df} \iff \frac{dV_{v,fz}}{dt} = \frac{dV_{v,df}}{dt} \sqrt{\frac{S_{v,fz}}{S_{v,df}}} \quad (9)$$

where  $df$  represents the flow driven by a deforming volume, and  $fz$  denotes the equivalent flow in the tube by keeping the initial length and diameter. The mass flow  $dV_{v,fz}/dt$  will be enforced in the tube.

### 2.3. Vein network modeling

A simple and fast numerical method was developed by decomposing the vein network into a set of hydrodynamic components. Fig. 5 illustrates how a local vein network in a pair of adjacent vertebrae was decomposed. The components were constructed according to their locations and functions. The component *Canal* concerns the IVVP located in the vertebral canal. The component *Canal joint* relates to the IVVP in the joint between the two vertebrae while the component *Branch*

corresponds to the IV. The EVVP is modeled in the component *External environment*. The vein network was implemented using SimHydraulics which is a toolbox of Matlab-Simulink.

2.3.1. Modeled hydraulic components

Fig. 6(a) illustrates the integrated block *Vein Vessel* that was established for computing the flow in the IVVP and IV tubes. The SimHydraulics block *Segmented Pipeline* is one of the elements of this integrated block. It models a tube composed of a number of segments as

$$p = \frac{1}{N} \frac{\rho h}{S_{v,jz}} \frac{dV_{v,jz}}{dt} - \frac{1}{N} \frac{\sqrt{\pi} f}{4} \frac{\rho h}{S_{v,jz}^{5/2}} \frac{dV_{v,jz}}{dt} \left| \frac{dV_{v,jz}}{dt} \right| \quad (10)$$

where  $\rho$  is density,  $\nu$  is kinematic viscosity, and  $N$  is number of the segments set as

10. The friction coefficient  $f$  is given by

$$f = \begin{cases} K_{sf}/Re, & Re \leq Re_L \\ f_L + \frac{f_T - f_L}{Re_T - Re_L} (Re - Re_L), & Re_L < Re < Re_T \\ \left\{ -1.8 \log \left[ 6.9/Re + \left( \frac{f}{7.4 \sqrt{S_{v,jz}/\pi}} \right)^{1.11} \right] \right\}^{-2}, & Re \geq Re_T \end{cases} \quad (11)$$

where  $Re = \frac{2}{\pi} \frac{dV_{v,jz}}{dt} S_{v,jz}^{-1/2} \nu^{-1}$ ,  $K_{sf}$  is shape factor set as 64. The hydraulic losses due to irregular shapes of the vein vessels were taken into account in the SimHydraulics block *Local Resistance* using a classical pressure-loss equation:

$$\Delta p = \begin{cases} K_l \frac{\rho}{2 S_{v,jz}^2} \frac{dV_{v,jz}}{dt} \left| \frac{dV_{v,jz}}{dt} \right|, & Re > Re_{cr} \\ K_l \frac{\pi Re_{cr} \nu}{4 S_{v,jz}^{3/2}} \frac{dV_{v,jz}}{dt}, & Re \leq Re_{cr} \end{cases} \quad (12)$$

where  $\Delta p$  is pressure loss,  $K_l$  is pressure loss coefficient, and  $Re_{cr}$  is the critical Reynolds number of flow transiting from laminar to turbulent status with the default value 150.  $K_l$  was specified as 1 for both of the direct and reverse flow. In addition to the volume changes in Eq. (8), the elasticity of the vein vessel walls can introduce wall deformations. This effect is modeled using the SimHydraulics block *Spring-Loaded Accumulator*

$$dV_{v,jz}/dp = K_{sc}, \quad (13)$$

where  $K_{sc}$  is set as  $1 \times 2.25^{-9} \text{ m}^3/\text{Pa}$  (Gelman, 2008).

Fig. 6(b) displays the subsystem constructed for modeling the local vein network surrounding a vertebra. The strategy of arranging the blocks is in accordance with the decomposed vein network shown in Fig. 5. The compensating flow, which is formulated in Section 2, is computed in the block *Compensating Flow*. By assuming that the compensating flow is distributed uniformly in the IVVP, a simple way to treat the flow is to add the block *Compensating Flow* between two identical tube segments, the blocks *Vein Vessel*. Because the length of the canal joint is shorter than that of the vertebral canal, we disregarded the compensating flow in the canal joint. The IV was modeled with the block *Vein Vessel* since unlike the IVVP it cannot be deformed by the canal volume change. The flow at the connection between the IVVP and IV was modeled using the SimHydraulics block *T-Junction*, which is formed by connecting three *Local Resistance* blocks.  $K_l$  is set as 2 for the connections linked to the IVVP and 4 for the connection linked to the IV. Whiplash motion has been assumed to have negligible impact on the blood flow in the EVVP. The SimHydraulics block *Constant Head Tank* was used to model the EVVP. Regarding free ambient

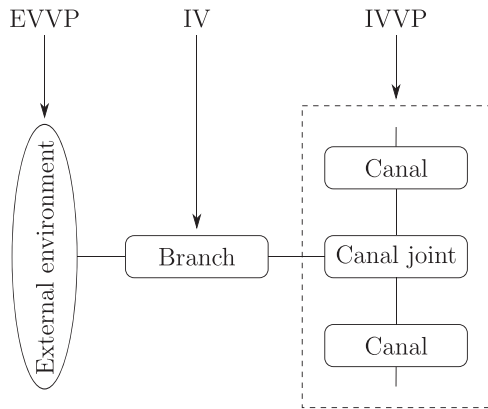


Fig. 5. Decomposition of the local vein network in a vertebra pair into a set of hydraulic components.

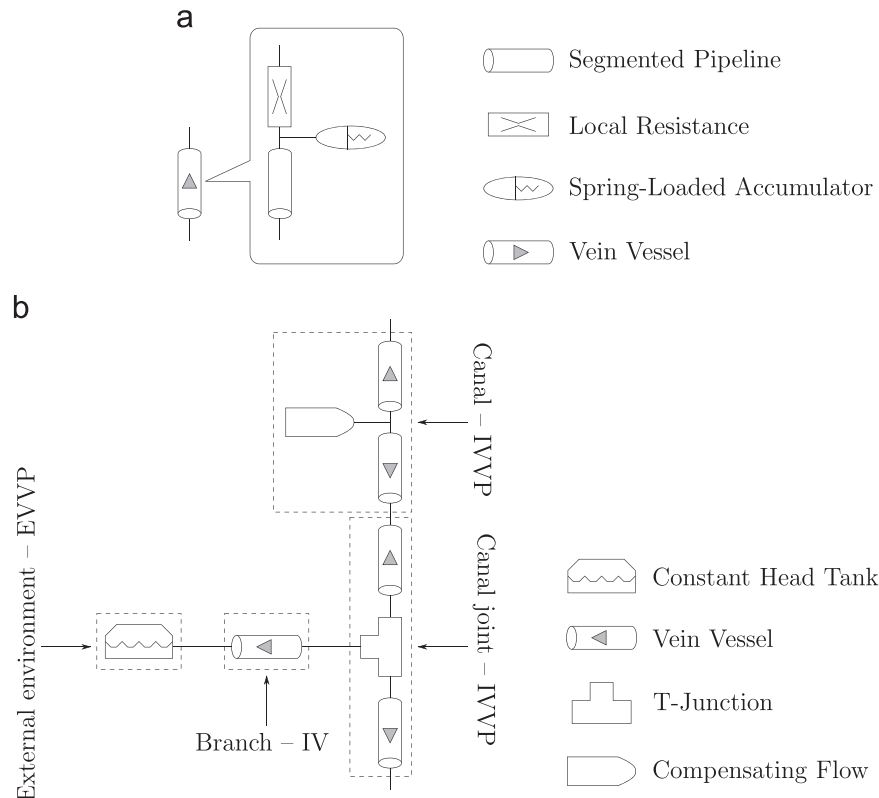


Fig. 6. The components of the hydrodynamic system: (a) the integrated block, *Vein Vessel*, modeling the veins; (b) the subsystem modeling the local vein network around a vertebra.

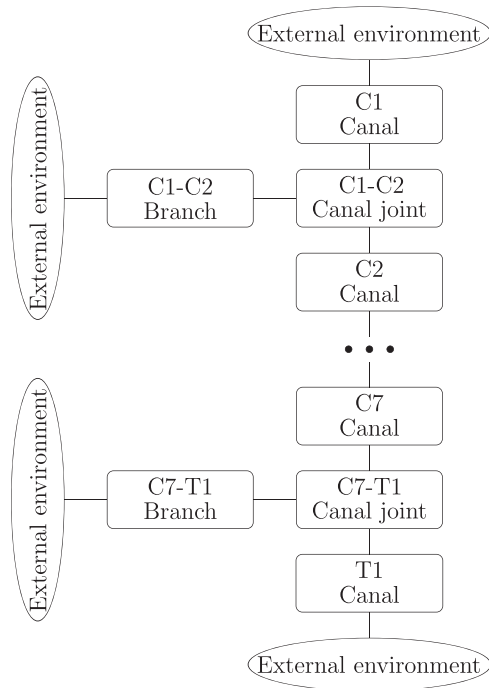


Fig. 7. The system established for modeling the entire vein network around the vertebrae from C1 to T1.

pressure in the EVVP, the pressure at the EVVP inlet is formulated as

$$p = \rho g H_f + K_f \frac{\rho}{2s^2} \frac{dV_{v,fz}}{dt} \left| \frac{dV_{v,fz}}{dt} \right| \quad (14)$$

where  $g$  represents the gravity, and  $H_f$  is fluid level in the tank with respect to the inlet position. To obtain negligible variations of  $H_f$  caused by inflow and outflow, the tank horizontal cross area is specified as  $10 \text{ m}^2$ . The flow is positive when it transports into the EVVP. The pressure loss coefficient  $K_f$  is set as 2.

The vertebrae of interest refer to the cervical vertebrae from C1 to C7 and the first thoracic vertebra T1. The local subsystem is identical for each of these vertebral levels. They were assembled to build a system that models the entire cervical vein network. Fig. 7 shows the system representing this entire vein network. With the assumption that pressure pulses can be absorbed in the skull and thoracic vertebral canal, the top and bottom sides of the system were connected to the external environment modeled with the SimHydraulics block *Constant Head Tank*.

2.3.2. Computational settings

The transverse vertebral dimensions of asymptomatic Chinese men and women reported by Lim and Wong (2004) were adopted here, namely, the mean values of the canal sagittal diameters and vertebral body AP diameters. The vertebral heights by Vasavada et al. (2008) were used, but are not listed for the sake of brevity.

The instant sagittal vertebral angulation angles are given with reference to the experiment by Ono et al. (2000). The cubic spline method (Schoenberg, 1969) is used to approximate the experimental data for the input. Fig. 8 shows the instant rotation angles. In Ono's experiment, the vertebrae from C2 to C6 were studied. However, the present system requires the rotation angles of C1, C7 and T1 as well. Since C1 is attached to C2, we made the simplified assumption that C1 rotates at the same angles as C2. Since the motion of the torso is generally not obvious (Adams and Dolan, 2005; Fice and Cronin, 2012), we assumed that C7 and T1 do not rotate.

Table 1 lists the parameters for the cases computed. The transverse vertebral dimensions are different in the B/L case and Case 2. The IVVP tube diameter is calculated by  $D_{ivvp} = c_{fd} r_d D_{c,BL}$ , where  $c_{fd}$  is an adjustable coefficient as the ratio of the venous blood volume to the canal volume,  $r_d$  is an empirical coefficient defined with  $D_{ivvp,BL}/D_{c,BL} = 0.14$ , and the subscript *BL* means the B/L case. This formulation implies the assumption that the volume of the venous blood contained in the IVVP tube is proportional to the canal volume. Based on Lim and Wong (2004), the ratio of  $D_c$  to its mean value varies between 0.965 and 1.035 for men and between 0.975 and 1.027 for women. Regarding these ratios,  $c_{fd}$  is set to 1 for the B/L case, 0.86 for Case 3, and 1.14 for Case 4. The adjustment of the vertebral heights is performed using the formulation  $h_c = c_{fh} h_{c,BL}$ . Vasavada et al. (2008) reported that for men and women  $h_c$  varies with ratios from 0.92 to 1.08 with respect to its mean value. To include the ratios, the adjustable coefficient  $c_{fh}$  is set to 0.8 for Case 5 and 1.2 for Case 6. As found by Stempier et al. (2003), the neck kinematics in women is greater than men. In addition, Carlsson et al. (2011, 2012) reported that the kinematics can also be intensified by increasing rear-end

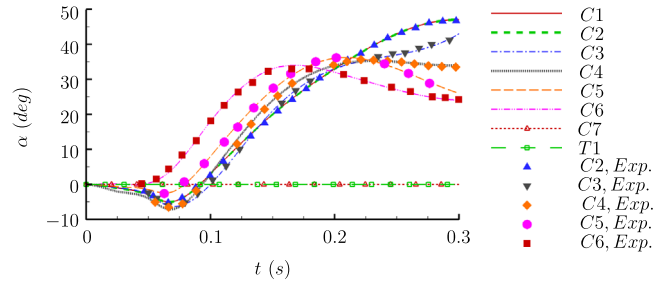


Fig. 8. The instant rotation angles of the vertebrae during whiplash motion with reference to the experimental data of Ono et al. (2000).

Table 1 The parameter settings for the system.

Case No.	Vertebra transverse dimension	$c_{fd}$ (%)	$c_{fh}$	$r_{kt}$ (%)	$r_{ka}$ (%)
B/L Case	Men, mean	1.96	1	100	100
Case 2	Women, mean	"	"	"	"
Case 3	"	1.44	"	"	"
Case 4	"	2.56	"	"	"
Case 5	"	"	0.8	"	"
Case 6	"	"	1.2	"	"
Case 7	"	"	0.8	80	"
Case 8	"	"	1.2	120	"
Case 9	"	"	0.8	"	75
Case 10	"	"	1.2	"	125

The ditto mark (") means the value of the B/L case is used.

$c_{fd}$  is the ratio of the venous blood volume to the canal volume.  $c_{fh}$  is defined to adapt the vertebral heights in terms of  $h_c = c_{fh} h_{c,BL}$ .

The vertebral transverse dimensions of women and men are set based on the mean values of the sagittal diameters of the vertebral canal and the AP diameters of the vertebral bodies for asymptomatic Chinese subjects reported by Lim and Wong (2004).

$r_{kt}$  is the factor for scaling the time of the input rotation angles of the vertebrae; and  $r_{ka}$  is the factor for scaling the amplitudes of the input rotation angles.

collision speed. To investigate the impact severity of the neck kinematics, the amplitudes and time of the vertebral rotation angles are scaled for the input. The factor  $r_{kt}$  is used to scale the time by 80% for Case 7 and 120% for Case 8.  $r_{ka}$  scales the amplitudes by 75% and 125% for Cases 9 and 10.

The density of blood is specified by  $1.06 \times 10^3 \text{ kg/m}^3$  (Kenner, 1989 for all the cases, and the kinematic viscosity  $3.3 \times 10^{-6} \text{ m}^2/\text{s}$  (Rosenson et al., 1996). Except for the parameters mentioned above, the other parameters for the SimHydraulics blocks use the default settings.

3. Results

Fig. 9(a) and (b) shows the pressures computed for the B/L case in comparison with the pressure at C4 in an anesthetized pig under whiplash exposure at the pulling force of 600 N (Svensson et al., 1993). The computed pressures are monitored at the positions where the integrated blocks of *Compensating Flow* are linked into the system shown in Fig. 6. The time of the experimental data was shifted backwards by 0.02 s to match the numerical results. The present computation uses the vertebral motions from Ono et al. (2000). Due to the difference in the starting times between Svensson's and Ono's experiments, it was decided to shift the timing. Another difference shown by the results is that the computed pressures in C5 and C6 match the experimental data in C4. Firstly, the difference is due to the different subjects between Svensson's and Ono's experiments. The vertebral anatomies of a pig and a human are similar (but not identical). Secondly, it is impossible to precisely and identically reproduce the vertebral motion of a human being in a pig model. In Svensson's results, the pressure transients were treated by excluding the ambient pressure, which was measured as the pig was not exposed to forces. In the computation, the ambient pressure is set to 0 Pa. Moreover, it is noteworthy that the experimental data shows a

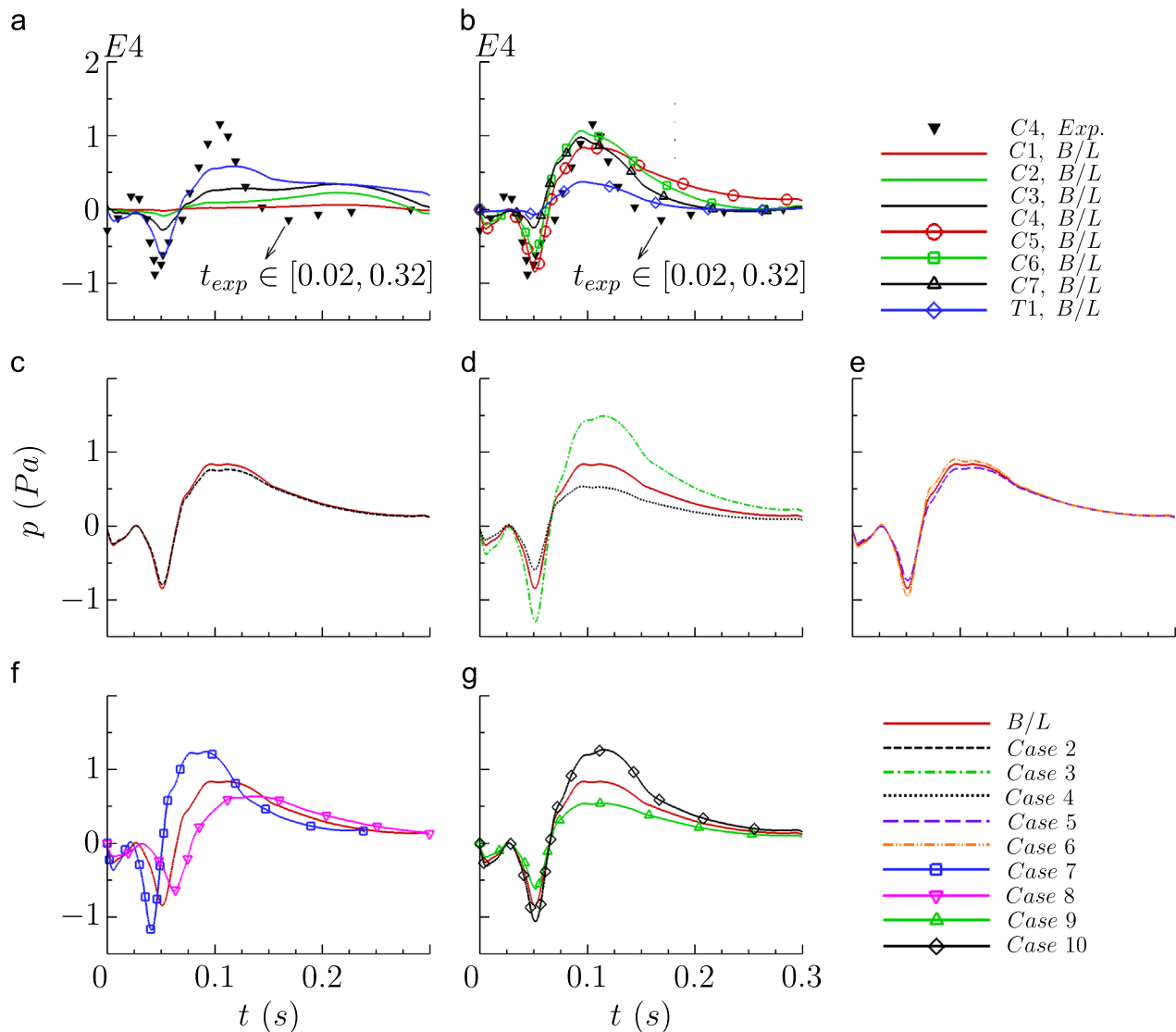


**Fig. 9.** (a) and (b) The pressure pulses of the venous blood in the IVVP in the B/L case, compared with experimental data of C4 with a pulling force of 600 N obtained by Svensson et al. (1993). Comparison of the pressure pulses in C5 for: (c) the B/L case and Case 2, where the transverse dimensions of the vertebrae are different in terms of the Chinese men and women; (d) the B/L case, Case 3 and Case 4, where the diameters of the IVVP tubes are variant; (e) the B/L case, Case 5 and Case 6, where the vertebral heights differ; (f) the B/L case, Case 7 and Case 8, where the time of the input rotation angles of the vertebrae is scaled by  $\pm 20\%$ ; (g) the B/L case, Case 9 and Case 10, where the amplitudes of the input rotation angles are scaled by  $\pm 25\%$ .

negative value at 0 s since small pressure fluctuations appear in the early stage. Nonetheless, the trends observed in the pig experiment were consistent with those found in the human being model. The first negative pressure dip appears in the very beginning. A second deeper dip reaches the minimum pressure at 0.05 s followed by a positive pressure crest reaching maximum pressure at 0.09 s.

Fig. 9(c) displays the pressure pulses in C5 for the B/L case and Case 2. The pressure magnitudes in Case 2 are lower than those in the B/L case. The reason is that the females possess smaller vertebral canal diameters and vertebral body AP diameters than the males. As shown in Eq. (5), small diameters lead to small  $l_v$ . The IVVP tube volume associated with  $l_v$  in Eq. (6) becomes small at the same rotation angles. Therefore, the pressure magnitudes caused by the volume changes are smaller in Case 2. However, a complete comparison of gender differences should include more geometrical details and kinematics.

Fig. 9(d) shows the pressures at C5 for the B/L case, Case 3 and Case 4. The effect of the diameter of the IVVP tube is examined by comparing the pressure pulses in these cases. A reduction of the pressure magnitudes is observed as the diameter increases. It

suggests that the percentage of venous blood in a vertebral canal influences the pressure magnitudes.

Fig. 9(e) displays the pressure pulses at C5 for the B/L case, Case 5 and Case 6. The pressure magnitudes reduce as the vertebral heights are increased. This reduction is however smaller than the reduction caused by increased IVVP tube diameter.

Fig. 9(f) shows the pressure pulses at C5 for the B/L case, Case 7 and Case 8. Scaling the time of the vertebral rotation angles by 80% leads to amplified pressure amplitudes.

Fig. 9(g) illustrates the pressure pulses at C5 for the B/L case, Case 9 and Case 10. The pressure amplitudes overall increase as a consequence of increased vertebral rotation angles.

#### 4. Discussion

Volume variations of the spinal canal during neck motion in whiplash exposure are likely accommodated by changes in IVVP blood volume. To model this effect, the present study presents a simple and fast numerical approach – a hydrodynamic system of

the cervical IVVP, IV and EVVP – using SimHydraulics. Based on the empirical formulations, the hydrodynamic components that constitute the system can model the main flow, which is one-dimensional along the tubes. The system is valid to predict the main flow in the way of adapting the parameters of the formulations. However, an apparent limitation of this modeling approach is that three-dimensional convection and dissipation of the real flow cannot be simulated.

The negative pressure in the IVVP leads to a low pressure environment inside the vertebral canal. Since the pressure in the EVVP outside the canal remains virtually unchanged, the pressure difference produces a suction effect for the venous blood. As indicated in Eq. (8), the suction corresponds to increased IVVP volume, which is caused by the flexion of the cervical spine. Accordingly, the positive pressure in the IVVP induces a squeezing effect for the venous blood since the IVVP volume is reduced by the spine extension.

The difference in averaged spinal canal diameter between females and males only produces a small difference in pressure magnitudes. Reducing the IVVP volume contained in the canal produces increased pressure magnitudes. However, the pressure amplitudes increase as a result of increased vertebral rotation angles. Besides, the pressure amplitudes can be amplified by accelerating the neck motion.

The computational results are compared with the pig experimental data (Svensson et al., 1993). The pig subject had a neck length and angular motion range that were representative of an adult human being. The pig neck was therefore considered as a qualitative model for this type of whiplash tests. The test sets allowed repeatable measurements with controlled parameter adjustments. The pig with the pulling force 600 N presented similar kinematics as the human subject sitting in a rigid seat without a head restraint (Ono et al., 2000), which is used as the computational input. An alternative is the PMHS tests of Eichberger et al. (2000). The tests were however performed with a head restraint that interrupted the neck motion. Their results were thus not comparable with Ono's data. Moreover, the properties of the soft tissues and blood would change postmortem. This adds uncertainties.

Improved data on tissue properties and dimensions would be needed to improve model accuracy. New whiplash experimental results that combine pressure monitoring and vertebral motion monitoring with well documented spinal geometrical details would be helpful for better validation of the model.

### Conflict of interest statement

The authors declare that we do not have any financial or personal relationship with other people or organizations that could have inappropriately influenced this study.

### Acknowledgments

The present work is funded by the Transport Area of Advance (AoA) of Chalmers University of Technology, Sweden. It was performed in association with SAFER (Vehicle and Traffic Safety Centre at Chalmers University of Technology).

### References

Adams, M.A., Dolan, P., 2005. Spine biomechanics. *J. Biomech.* 38 (10), 1972–1983.  
 Alastruey, J., Parker, K.H., Sherwin, S.J., 2012. Arterial pulse wave haemodynamics. In: proceedings of the 11th International Conference on Pressure Surges, Virtual PiE Led t/a BHR Group, pp. 401–442.  
 Aldman, B., 1986. An analytical approach to the impact biomechanics of head and neck. In: The 30th Annual Proceedings of Association for the Advancement of Automotive Medicine, pp. 439–454.

Batson, O.V., 1940. The function of the vertebral veins and their role in the spread of metastases. *Ann. Surg.* 112 (1), 138–149.  
 Batson, O.V., 1957. The vertebral vein system. *Am. J. Roentgenol.* 78, 195–212.  
 Breig, A., 1978. Arterial mechanical tension in the central nervous system. Almqvist & Wiksell, Stockholm.  
 Breschet, G., 1819. *Essai sur les veines der rachis*. Mequigon-Morvith, Paris.  
 Cairns, B.E., Arendt-Nielsen, L., Sacerdote, P., 2015. Perspectives in pain research 2014: neuroinflammation and glial cell activation: the cause of transition from acute to chronic pain? *Scand. J. Pain* 6, 3–6.  
 Carlsson, A., Linder, A., Davidsson, J., Hell, W., Schick, S., Svensson, M.Y., 2011. Dynamic kinematic responses of female volunteers in rear impacts and comparison to previous male volunteer tests. *Traffic Inj. Prev.* 12 (4), 347–357.  
 Carlsson, A., Siegmund, G.P., Linder, A., Svensson, M.Y., 2012. Motion of the head and neck of female and male volunteers in rear impact car-to-car impacts. *Traffic Inj. Prev.* 13, 378–387.  
 Curatolo, M., Bogduk, N., Ivancic, P.C., McLean, S.A., Siegmund, G.P., Winkelstein, B. A., 2011. The role of tissue damage in whiplash-associated disorders: discussion paper 1. *Spine* 36, 309–315.  
 Eichberger, A., Darok, M., Steffan, H., Leinzinger, P.E., Boström, O., Svensson, M.Y., 2000. Pressure measurements in the spinal canal of postmortem human subjects during rear-end impact and correlation of results to the neck injury criterion. *Accid. Anal. Prev.* 32, 251–260.  
 Estes, M.S., McElhaney, J.H., 1970. Response of brain tissue of compressive loading. In: *The Spine, Proceedings of the 4th ASME Biomechanics Conference*.  
 Fice, J.B., Cronin, D.S., 2012. Investigation of whiplash injuries in the upper cervical spine using a detailed neck model. *J. Biomech.* 45 (6), 1098–1102.  
 Gelman, S., 2008. Venous function and central venous pressure. *Anesthesiology* 108 (4), 735–748.  
 Gustafsson, M., Stigson, H., Krafft, M., Kullgren, A., 2015. Risk of permanent medical impairment (RPMI) in car crashes correlated to age and gender. *Traffic Inj. Prev.* 16 (4), 353–361.  
 Jonsson, B., 2008. Interaction between humans and car seats – studies of seat adjustments and occupant posture and its possible connection to real world neck injuries in rear-end impacts (Ph.D. thesis). Department of Surgery and Perioperative Science, Umeå University, Sweden.  
 Kenner, T., 1989. The measurement of blood density and its meaning. *Basic Res. Cardiol.* 84 (2), 111–124.  
 Lim, J.K., Wong, H.K., 2004. Variation of the cervical spinal torg ratio with gender and ethnicity. *Spine J.* 4, 396–401.  
 Löfgren, L., von Essen, C., Zvetnov, N.N., 1973. The pressure-volume curve of the cerebrospinal fluid space in dogs. *Acta Neurol. Scand.* 49, 557–574.  
 Moore, K.L., Agur, A.M.R., Dalley, A.F., 2013. Contents of vertebral canal, Clinically oriented anatomy, 7th edition. Lippincott Williams and Wilkins, Philadelphia, pp. 621–629.  
 Ono, K., Kaneoka, K., Inami, S., 2000. Analysis of seat properties on human cervical vertebral motion in low-speed rear-end impacts. In: Yoganandan, N., Pintar, F.A. (Eds.), *Frontiers in Whiplash Trauma: Clinical and Biomechanical*. IOS Press, Amsterdam, pp. 372–388.  
 Örtengren, T., Hansson, H.A., Lövsund, P., Svensson, M.Y., Suneson, A., Säljö, A., 1996. Membrane leakage in spinal ganglion nerve cells induced by experimental whiplash extension motion: a study in pigs. *J. Neurotrauma* 13 (3), 171–180.  
 Panjabi, M.M., 2006. A hypothesis of chronic back pain: ligament subfailure injuries lead to muscle control dysfunction. *Eur. Spine J.* 15, 668–676.  
 Parke, W.W., 1992. Applied anatomy of the spine. In: Rothman, R.H., Simeone, F.A. (Eds.), *The Spine*. W.B. Saunders, Philadelphia, pp. 35–88.  
 Penning, L., 1995. Kinematics of cervical spine injury: a functional radiological hypothesis. *Eur. Spine J.* 4, 126–132.  
 Rosenson, R.S., McCormick, A., Uretz, E.F., 1996. Distribution of blood viscosity values and biochemical correlates in healthy adults. *Clin. Chem.* 42 (8), 1189–1195.  
 Schoenberg, I.J., 1969. Approximations with Special Emphasis on Spline Functions. Academic Press, New York.  
 Siegmund, G.P., Wheeler, J.B., Brault, J.R., 1998. Volume changes in the human cervical spinal canal between the neutral and retracted head positions. In: *Proceedings of Whiplash '98 Symposium*, Phoenix, AZ, November 5–6.  
 Siegmund, G.P., Winkelstein, B.A., Ivancic, P.C., Svensson, M.Y., Vasavada, A., 2009. The anatomy and biomechanics of acute and chronic whiplash injury. *Traffic Inj. Prev.* 10, 101–112.  
 Stemper, B.D., Yoganandan, N., Pintar, F.A., 2003. Gender dependent cervical spine segmental kinematics during whiplash. *J. Biomech.* 36 (9), 1281–1289.  
 Svensson, M.Y., 1993. Neck-injuries in rear-end car collisions – sites and biomechanical causes of the injuries, test methods and preventive measures (Ph.D. thesis). Chalmers University of Technology, Sweden.  
 Svensson, M.Y., Aldman, B., Boström, O., Davidsson, J., Hansson, H.A., Lövsund, P., Säljö, A., 1998. Nerve cell damages in whiplash injuries: animal experimental studies. *Der Orthopäde* 27 (12), 820–826.  
 Svensson, M.Y., Aldman, B., Hansson, H.A., Lövsund, P., Seeman, T., Suneson, A., Örtengren, T., 1993. Pressure effects in the spinal canal during whiplash extension motion – a possible cause of injury to the cervical spinal ganglia. In: *International Research Council on the Biomechanics of Injury*, Eindhoven, Netherlands, pp. 189–200.  
 Taylor, J.R., 2002. The pathology of whiplash: neck sprain. *B. C. Med. J.* 44 (5), 252–256.  
 Vasavada, A.N., Danaraj, J., Siegmund, G.P., 2008. Head and neck anthropometry, vertebral geometry and neck strength in height-matched men and women. *J. Biomech.* 41 (1), 114–121.